

Estimation of deepwater temperature and hydrogeochemistry of springs in the Takab geothermal field, West Azerbaijan, Iran

Reza Sharifi · Farid Moore · Zargham Mohammadi · Behnam Keshavarzi

Received: 10 October 2014 / Accepted: 8 December 2015 / Published online: 5 January 2016
© Springer International Publishing Switzerland 2015

Abstract Chemical analyses of water samples from 19 hot and cold springs are used to characterize Takab geothermal field, west of Iran. The springs are divided into two main groups based on temperature, host rock, total dissolved solids (TDS), and major and minor elements. TDS, electrical conductivity (EC), Cl^- , and SO_4^{2-} concentrations of hot springs are all higher than in cold springs. Higher TDS in hot springs probably reflect longer circulation and residence time. The high Si, B, and Sr contents in thermal waters are probably the result of extended water–rock interaction and reflect flow paths and residence time. Binary, ternary, and Giggenbach diagrams were used to understand the deeper mixing conditions and locations of springs in the model system. It is believed that the springs are heated either by mixing of deep geothermal fluid with cold groundwater or low conductive heat flow. Mixing ratios are evaluated using Cl, Na, and B concentrations and a mass balance approach. Calculated quartz and chalcedony geothermometer give lower reservoir temperatures than cation geothermometers. The

silica-enthalpy mixing model predicts a subsurface reservoir temperature between 62 and 90 °C. The $\delta^{18}\text{O}$ and δD ($\delta^2\text{H}$) are used to trace and determine the origin and movement of water. Both hot and cold waters plot close to the local meteoric line, indicating local meteoric origin.

Keywords Geothermometry · Isotope · Hydrogeochemistry · Takab geothermal field

Introduction

Numerous thermal and cold springs are located in active volcanic regions all over the world as a result of eruptive events, as well as obvious manifestations of long-lived hydrothermal systems.

Considerable research has studied the origins of geothermal water and hydrogeochemical processes in these waters. Hydrogeochemical indicators, such as major ion ratios, can be used to study recharge origin and mixing behavior of thermal water (Vengosh et al. 2002).

Physico-chemical data in geothermal aquifers can also indicate structural elements of geothermal systems (Favara et al. 2001). These approaches can help characterize water–rock interaction processes as thermal waters flow through various strata and the geochemical evolution of groundwater under different flow conditions (Larsen et al. 2001). Geothermal fluids have diverse chemical characteristics, which largely reflect their geological setting. Many of these chemical differences largely depend on the source of recharge water and the contribution of gases from magmatic or

R. Sharifi (✉) · F. Moore · Z. Mohammadi · B. Keshavarzi
Department of Earth Sciences, Faculty of Sciences, Shiraz
University, Shiraz, Iran
e-mail: rezasharifi@shirazu.ac.ir

F. Moore
e-mail: moore@susc.ac.ir

Z. Mohammadi
e-mail: zmohammadi@shirazu.ac.ir

B. Keshavarzi
e-mail: bkeshavarzi@shirazu.ac.ir

metamorphic sources. Temperature sensitive equilibria between minerals, geothermal solutions, and in some cases a vapor phase can affect the chemical composition of a geothermal fluid, providing the basis for chemical geothermometry. Chemical geothermometers are normally applied to thermal springs, steam vents, and geothermal wells for inferring reservoir temperatures in geothermal exploration and exploitation. The most widely used geothermometers are based on silica (quartz and chalcedony) and cation ratios (mainly Na/K and Na-K-Ca). Others that have been developed are based on Na/Li, Li/Mg, K/Mg, Ca/Mg, Na/Ca, and K/Ca ratios and Na-K-Mg relationships. Moreover, the geothermometer using the fractionation of oxygen isotopes between water and dissolved sulfate is also tested. Iran is located in an active tectonic belt, namely, the Alpine–Himalayan orogenic belt, with many tectonic structures including grabens, active fault systems, volcano-hydrothermal alteration zones, and geothermal areas. The Takab geothermal field is located northwest of Iran and is an important tourist resort with many remarkable thermal springs that

have been used for bathing and medicinal purposes for several years (Fig. 1). Several surveys have already been carried out in this area (Modabberi and Moore 2004; Karimzadeh Somarin and Lentz 2008; Azizi and Moinevaziri 2009; Saki 2010; Naderi 2013). The studies mainly deal with geological, petrological, environmental, and tectonical characteristics of the area. However, the thermal and cold springs of the Takab area are yet to be studied considering their hydrogeochemical and isotopic characteristics. The aim of the present study is to describe the hydrochemistry of the hot and cold springs of the Takab geothermal field, the mixing of geothermal fluids with cold fresh water, estimate reservoir temperatures, and to determine the isotopic characteristics in order to infer the source of the thermal waters.

Tectonic and geological setting

The Takab area lies at the boundary of the Urumieh-Dokhtar volcanic arc and the Sanandaj-Sirjan

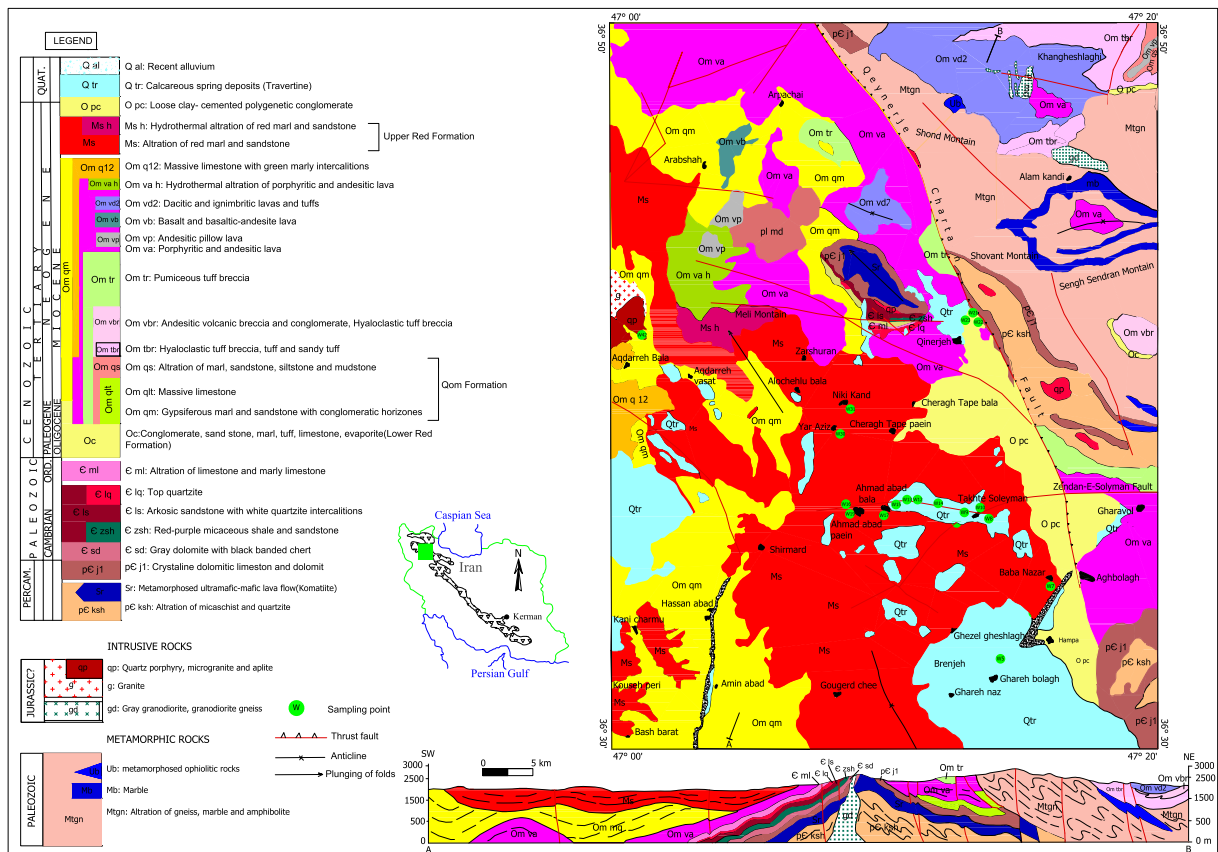


Fig. 1 Geological map and sampling site of Takab geothermal area (modified after GSI 1999)

volcano sedimentary zone, both of which extend over 2000 km in a NW-SE direction parallel to the Zagros thrust fault (Sharifi et al. 2014). The area has experienced repeated cycles of orogenic activity, including structural uplift, sedimentation, magmatism, and metamorphism (Daliran et al. 2013). The geological formations mostly comprise Precambrian metamorphics, Tertiary volcanics, and Quaternary sediments. Syn-extensional intra-arc faulting along reactivated crustal structures created a graben basin in the subsiding Takab block in Oligo-Miocene time (Daliran 2008). The graben basin of Takab is filled with continental to shallow marine sediments of Oligo-Miocene to recent age (Fig. 1). Sedimentation was accompanied by syn-extensional high-level magmatism (Stockli et al. 2004), volcanic activity, and hydrothermal mineralization. The Takab basin is underlain by basement rocks that comprise metamorphosed pelite, psammite, carbonate, and mafic volcanic rocks of Upper Proterozoic to Lower Cambrian age and unmetamorphosed Cambrian to Ordovician formations. In the Takab basin, the Lower Red Formation directly overlies the basement rocks and is part of an extensive Oligocene unit in Iran that comprises a transgressive continental red bed sequence of basal conglomerate, sandstone and marl, and evaporite sediments (Boni et al. 2007). The Lower Red Formation grades upward into the Qom Formation comprising fine-grained detrital sediments with marl, tuff, and limestone that is locally reefal. The Upper Red Formation overlies the Qom Formation and comprises red marl and sandstone with gypsum beds. A major northwest-southeast trending fault puts the Precambrian metamorphics in juxtaposition with the Tertiary rocks in the middle of the area (e.g., at Qinerjeh field) (Fig. 1). Cenozoic sediments of the Takab basin comprise widespread gravel fans, alluvium, and very extensive travertine deposits that are related to numerous low to moderately hot springs in the area. The location of the thermal springs is commonly controlled by faults. Thermal springs continue to precipitate travertine and mud deposits that locally contain about 1.62 wt.% As, 22 wt.% Cu, 14 wt.% Se, 1160 ppm Au, and 1920 ppm Ag as well as strong enrichments in Ba, Sb, Pb, Hg, Te, Ge, Bi, and Ni (Daliran 2003). Most travertines are located to the west of the Qeynarjeh-Chartagh fault, on the gypsiferous Upper Red Formation of the Takab depression, and follow 55° (NE-SW), 90° (E-W), and 120° (NW-SE) striking structures. Examples are the large Berenjeh travertine

field with a length of 3 km, a width of 1.7 km, and a thickness of at least 200 m, and the E-W trending, 4 km long, and 1.3 km wide Zendan travertine field with many still active hot springs near Ahmad abad as well as the remarkable 110-m high Zendane-Soleiman travertine mound (Fig. 1). Minimum and maximum elevations in the study area are about 1785 and 2955, respectively, with an average of 2650 m above mean sea level. The mean annual precipitation is 300 mm in the Takab area. The aquifers are fed by infiltration of annual rainfall. At high elevation, snow predominates and contributes to the recharge processes during late spring. There are several springs as discharging points of the aquifers (Fig. 1). The general flow direction follows topographic slope. Discharge value of the springs range from less than 1 l/s to maximum 100 l/s (Table 1). The large number of springs and their low discharge value could be considered an indication of the effect of the faults on the groundwater circulation.

Material and methods

Water samples including hot and cold springs were collected in September 2012. The locations of the water samples are shown in Fig. 1. All samples were collected in high-density polyethylene bottles. One-hundred-twenty-milliliter samples acidified with 2 ml of 65 % HNO₃ was collected for cation analyses, while 1000 ml samples was collected for anion analyses. Before acidification, the samples were filtered with a 0.45- μ m pore size membrane. The discharge temperature (*T*), pH, Eh, total dissolved solids (TDS), and electrical conductivity (EC) were measured using portable instruments (Eutech instruments, PCD650) in the field. Separate batches of 120 ml samples were collected for oxygen and hydrogen isotope analyses. Anions were determined using ion chromatography (Dionex model 2010i) on an unacidified aliquot. SO₄²⁻, HCO₃⁻, and Cl⁻ were determined by spectrophotometry (T80 UV-Vis Spectrophotometer PG Instrument Ltd.), titration, and Mohr's method, respectively. Major ion and trace element concentrations in the water samples were determined using inductively coupled plasma-mass spectrometry (ICP-MS) at Acme Analytical Laboratories Ltd., accredited under ISO 9002, Canada, using a Perkin Elmer model Elan 6000 instrument.

Stable isotope analyses of water samples were carried out at the Helmholtz Centre for Environmental Research

Table 1 Chemical and isotopic composition of water samples from Takat geothermal field

Sample	Elevation (m)	Discharge (L s ⁻¹)	pH	Eh (mV)	T (°C)	EC (μS cm ⁻¹)	TDS (mg L ⁻¹)	Ca ²⁺ (mg L ⁻¹)	Mg ²⁺ (mg L ⁻¹)	Na ⁺ (mg L ⁻¹)	K ⁺ (mg L ⁻¹)
W31	1999	2	6.87	225.8	11.5	651.4	281.6	110.21	24.31	7.36	1.56
W9	2297	15	7.12	250.9	11.8	825.1	363	136.27	64.41	13.1	4.69
W7	2193	40	7.63	225	12.2	270	120.4	55.11	6.08	33.34	0.78
W16	1929	4	7.27	176.3	12.5	549.2	252.1	90.18	36.46	8.51	1.17
W2	2160	2	7.69	206.3	13.6	353.8	171.4	67.13	12.15	5.06	0.78
W10	2192	3	7.17	259.5	13.8	321.6	154.4	70.14	3.65	20	0.78
W5	2143	3	7.48	220.2	13.9	531.8	243.8	80.16	30.38	8.97	1.17
W30	1854	7	6.2	89.5	14.4	4462	2160	547.06	117.88	423.02	65.68
W19	1981	2	6.86	193.9	14.8	1476	758.6	230.45	66.84	61.61	3.52
W42	2121	0.5	6.27	-185.9	20.4	4025	2435	761.48	227.86	243.46	36.36
W17	2022	2	6.87	152.4	20.1	2303	1360	500.98	60.76	71.73	5.47
W8	2224	100	6.95	264.9	21.2	973.4	696.3	176.34	63.19	10.81	4.69
W15	2047	3	6.14	-190.9	27.1	2779	2632	651.27	60.76	70.12	6.26
W14	2199	5	6.7	-15.2	28.9	2836	2805	651.27	91.14	80.47	6.26
W13	2127	15	6.61	-113.5	29.3	2587	2587	535.04	76.56	71.73	23.46
W12	2128	35	6.18	-228.5	38.2	2245	3612	591.15	99.65	71.73	20.72
W22	2261	20	6.45	198.7	28.2	945.9	918.6	190.37	38.89	15.17	2.35
W23	2329	5	5.98	-105.4	34.8	1181	1342	280.55	48.61	15.17	2.35
W21	2342	30	6.12	95.7	39.4	1232	1773	248.48	35.24	17.47	2.35

Sample	HCO ₃ ⁻ (mg L ⁻¹)	SO ₄ ²⁻ (mg L ⁻¹)	Cl ⁻ (mg L ⁻¹)	B (μg L ⁻¹)	As (μg L ⁻¹)	Si (μg L ⁻¹)	Sr (μg L ⁻¹)	SiO ₂ (mg L ⁻¹)	δ ¹⁸ O (‰SMOW)	δ ² H (‰SMOW)
W31	396.43	40.1	19.5	466.43	1.02	N/D	N/D	N/D	N/D	N/D
W9	567.2	86.96	21.27	494	341.5	8831	734.7	21	N/D	N/D
W7	243.96	14.49	12.41	20	110.69	4135	115	8.84	-9.22	-57.15
W16	365.93	65.7	17.73	2347	0.15	9632	1356	20.6	N/D	N/D
W2	253.1	9.66	8.86	9.83	24.45	N/D	N/D	N/D	N/D	N/D
W10	262.25	10.63	7.09	12.95	0.85	N/D	N/D	N/D	N/D	N/D
W5	365.93	29.47	8.86	45.73	5.56	N/D	N/D	N/D	N/D	N/D
W30	2287.08	96.62	857.96	40.444	27.46	15895.28	2678.97	34	-8.8	-59.61
W19	658.68	386.48	39	N/D	150.71	N/D	N/D	N/D	N/D	N/D
W42	2866.48	325.61	460.89	41.879	24.95	16.828	3992	36	N/D	N/D
W17	1067.31	652.19	31.91	5228	628.59	16.410	2377	35.1	N/D	N/D
W8	762.36	43.48	14.18	438	250.18	7482	521	17	-9.8	-59.92
W15	1616.21	591.8	63.82	6737	131.39	N/D	3161	N/D	N/D	N/D

Table 1 (continued)

Sample	HCO ₃ ⁻ (mg L ⁻¹)	SO ₄ ²⁻ (mg L ⁻¹)	Cl ⁻ (mg L ⁻¹)	B (μg L ⁻¹)	As (μg L ⁻¹)	Si (μg L ⁻¹)	Sr (μg L ⁻¹)	SiO ₂ (mg L ⁻¹)	δ ¹⁸ O (‰SMOW)	δ ² H (‰SMOW)
W14	1536.92	700.5	60.27	7193	291.43	N/D	3404	N/D	N/D	N/D
W13	1628.4	396.14	88.63	N/D	365.22	17765.31	N/D	38	N/D	N/D
W12	1860.16	362.81	70.91	6914	152.02	16.555	3263	35	-10.23	-63.25
W22	670.88	59.42	35.45	809	491.68	9639	312.1	24	N/D	N/D
W23	1067.31	77.3	35.45	1332	564.71	13.421	653.5	28	N/D	N/D
W21	853.84	69.57	24.82	1341	986.43	13.232	482.3	29	-10.35	-63.12

Isotopic data for the water samples collected in September 2012

N/D not measured

(UFZ), Germany, using an IR MS Delta S mass spectrometer and EQ measuring method against the V-SMOW standard. The analytical errors of the δ¹⁸O and δ²H measurements are 0.1 and 0.5 ‰, respectively. Charge-balance error of the waters is less than 5 %, which is within the limits of acceptability. Mineral saturation indices for a number of common minerals potentially present in the studied localities were calculated at measured discharge temperatures by PHREEQC (Parkhurst and Appelo 1999) interfaced with AquaChem 5.0. Also, the geochemical modeling program Visual MINTEQ (version 2.2, a recent adaption of the original code written by Allison et al. (1991)) and RockWare Aq.QA computer code (version 1.1) were used to calculate the activity of species in the water samples and geothermometry, respectively.

Result and discussion

Hydrogeochemical properties of water samples

This study is based on samples from ten hot ($T > 20\text{ }^{\circ}\text{C}$) and nine cold ($T < 20\text{ }^{\circ}\text{C}$) springs in this area. Chemical composition of all samples is shown in Table 1, and their locations are presented in Fig. 1. The composition of hydrothermal water depends on many factors, of which temperature-dependent reactions between host rock and water are a major factor. Leaching also plays an important role when the amount of a particular constituent is too small to achieve equilibrium. However, mixing, boiling, and cooling processes usually have a pronounced influence on the final composition of geothermal waters (Warner et al. 2013). Most hot springs are slightly acidic and may be divided into two main groups on the basis of their host rock, temperature, and chemistry. The first group comprises hot water samples from Takhte-Soleyman (W8, W12, W13, W14, W15, and W17) and Aqdarreh (W42) fields with sedimentary and volcanic host rocks. The temperatures range from 20.1 to 38.2 °C), with Ca²⁺ (~176–761 mg/L); SO₄²⁻ (~43.4–700.5 mg/L); HCO₃⁻ (~762–2866 mg/L); and high Cl⁻ (14–460 mg/L), B (438–41,879 μg/L), Si (7482–17765.31 μg/L), and Sr (521–3992 μg/L) contents (Table 1). The second group is Qinerjeh field (W21, W22, and W23). In contrast to the first group, these hot waters have higher temperature (28.2–39.4 °C) and ascend through metamorphic host rocks. Also, they contain lower Si, Sr, and B contents than the first group.

The cold springs are also divided into two main groups. The first group (W2, W5, W7, W9, W10, W16, and W31) is characterized by cold ($T=11.5$ to 13.9 °C), low TDS (~ 120 – 363 mg/L), and slightly acidic to neutral (~ 6.8 – 7.69 pH) water that contains Ca^{2+} (~ 55 – 136.27 mg/L), SO_4^{2-} (~ 9.6 – 86.96 mg/L), and HCO_3^- (~ 244 – 567 mg/L) and low Cl^- (7 – 21.27 mg/L) content. The springs originate from the sedimentary and travertine formations in the Takhte-Soleyman field. The second group (W19 and W30) contains higher values of T (14.4 – 14.8 °C), TDS (~ 758 – 2160 mg/L), SO_4^{2-} (~ 96.6 – 386.4 mg/L), HCO_3^- (~ 658 – 2287 mg/L), and Cl^- (~ 39 – 857 mg/L) contents. The hydrochemical characteristics of various waters are presented in Table 1 and Fig. 2. The hot and cold springs are plotted in rather distinct fields. Apart from samples W19 and W30, whose relatively high sulfate and Cl compositions are likely due

to contact with gypsum-rich Oligo-Miocene evaporites, all cold waters lie near the HCO_3^- corner, being derived from carbonate-hosted deposits. Hot spring samples are broadly Ca (SO_4)- HCO_3^- type and Ca- SO_4 (W15 and W17) type, whereas Ca- SO_4 - HCO_3^- type is the main water type in cold springs. Other water types such as Ca (SO_4)-Cl- HCO_3^- type (W42) and Ca-Cl type (W30) are also present. TDS, EC, Cl^- , and SO_4^{2-} concentrations of hot springs are all higher than in cold springs, with mean TDS of 2016.09 and 500.59 mg/L for hot and cold springs, respectively. Higher TDS in hot springs probably reflect longer circulation and residence time. In the Takhte-Soleyman field, water flows through sedimentary formations. This is likely responsible for the higher Ca^{2+} and SO_4^{2-} in these waters. The variable ion content of cold springs (Fig. 2) is probably due to the different degrees of mixing between cold and hot waters at depth.

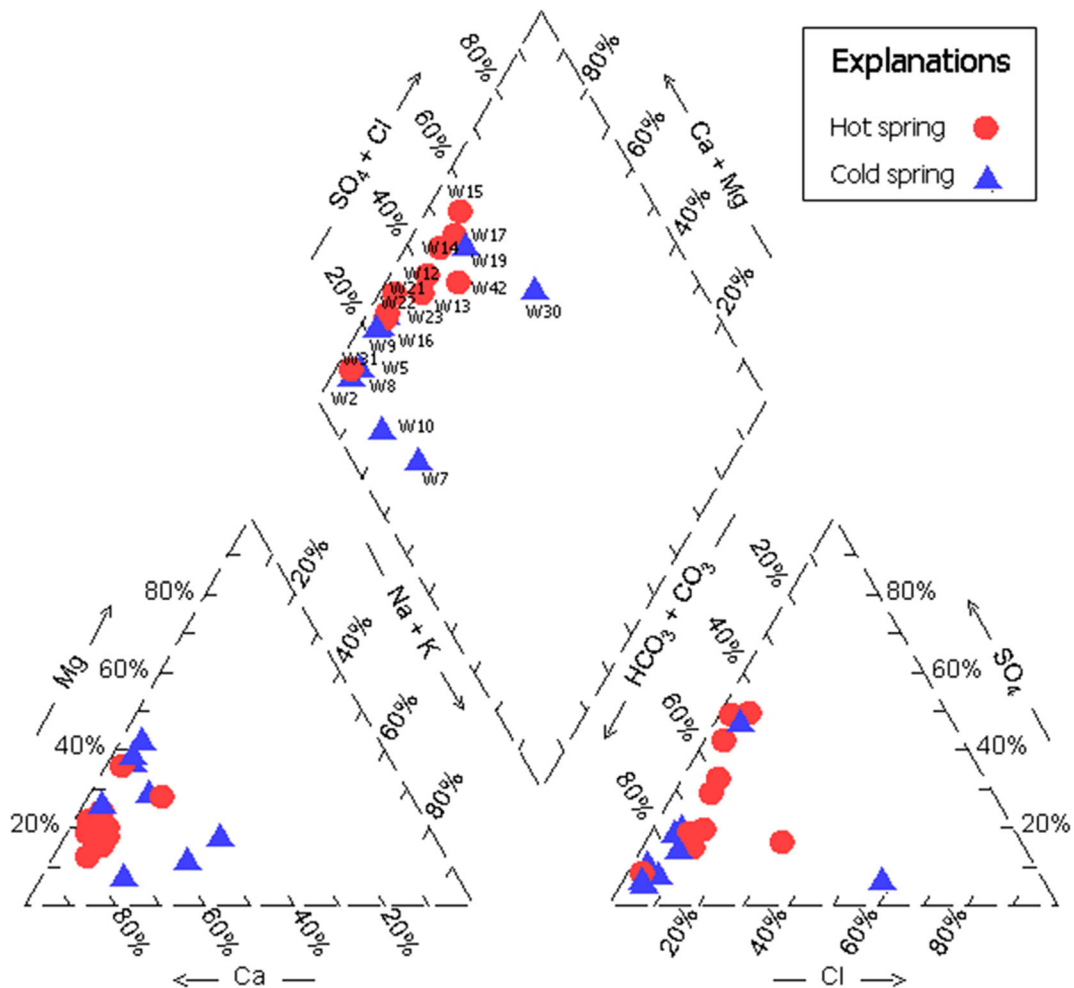


Fig. 2 Distribution of hot and cold springs from the study area in the Piper diagram

Major and minor elements

Major ion composition and ionic ratios can act as a track record of water–rock interaction during flow (Möller et al. 2007). The concentrations of some major ions and ionic ratios were plotted against chloride, which is regarded as a conservative element (Fig. 3). A wide range of concentrations is observed; hence, Cl^- is expressed in logarithmic form. Increases in Na and K versus Cl in hot springs (Fig. 3a, b) almost certainly reflect progressive reaction with feldspars or clay minerals at depth and thus may be used as an independent indicator of residence time. Apparently, hot springs take part in a much longer, deeper, regional flow path than

cold springs and so have much higher Na/Cl and K/Cl ratios than cold springs. Dissolution of calcite and/or dolomite, along with weathering of Ca-bearing plagioclase, can explain the relatively high Ca/Cl ratios in hot water. On the other hand, low Ca/Cl ratios in cold water (Fig. 3c) probably reflect calcite precipitation along the flow path. Hot spring calculated saturation index (SI) is at or above calcite saturation (Table 3). Figure 3d shows a positive correlation between Mg and Cl. In high-temperature thermal systems, Mg is incorporated into secondary alteration minerals by ion exchange reactions, resulting in very low Mg levels (Nicholson 1993). Since the Cl concentration of water from the deep reservoir is generally high, a negative correlation

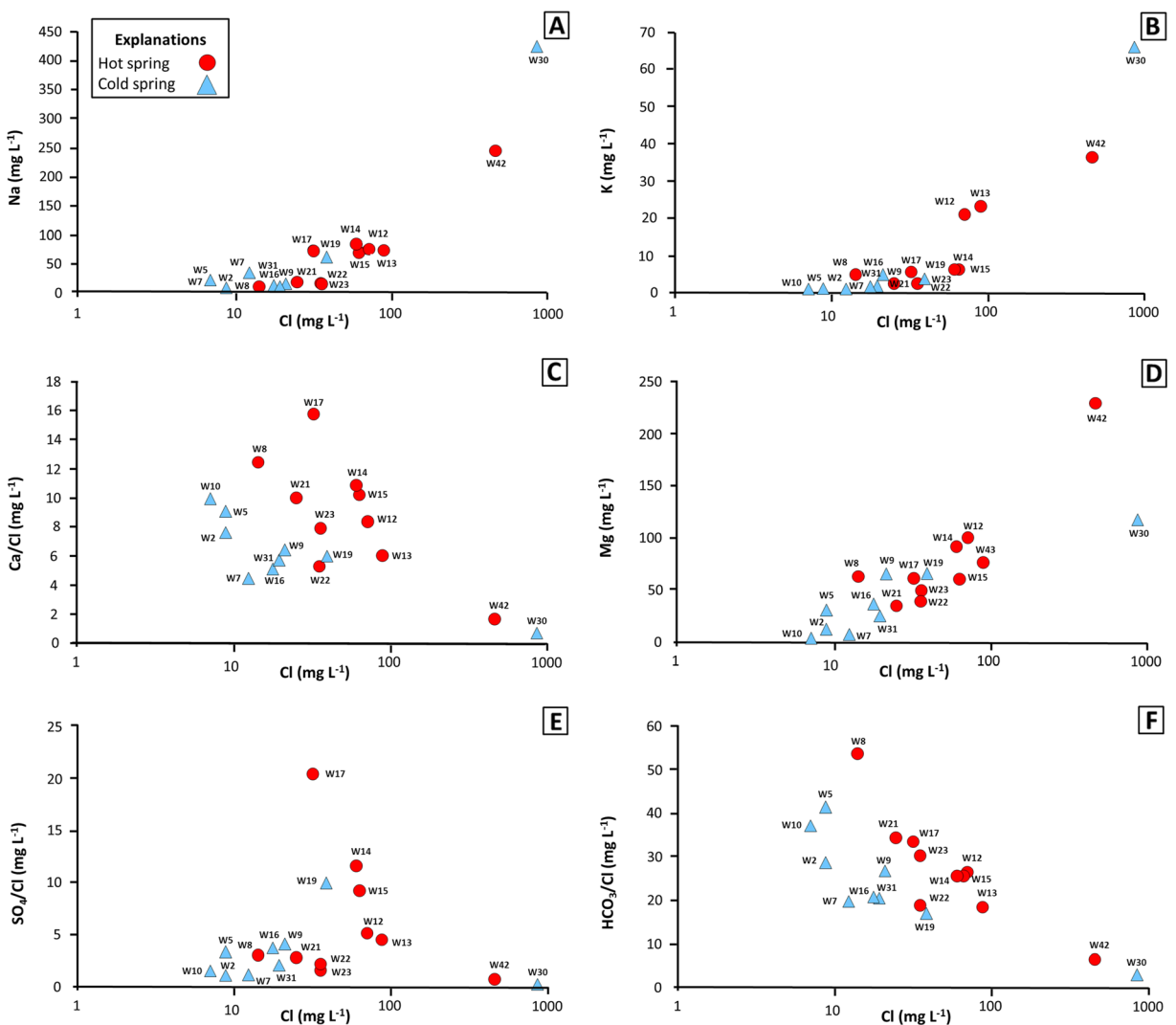


Fig. 3 Plots of ions (a, b) and ion ratios (c–f) versus chloride concentration for various water samples in Takab geothermal area.

Hot spring (red circle) and cold spring (blue triangle). (Color figure online)

is expected between Cl and Mg. However, a positive correlation or high concentrations of Mg indicate that the ascending hot water is mixed with cold water (Fig. 3d). SO_4/Cl ratio is also higher in hot springs (Fig. 3e). The higher and similar SO_4 and Cl content in hot springs is distinctive (Table 1) and suggests a common source. SO_4 is close to equilibrium with respect to gypsum, and concentrations in both geothermal fields increase until saturation is almost reached (Table 3). Relatively higher HCO_3/Cl ratios in cold springs reflect shorter flow path and hence faster circulation, while lower HCO_3/Cl ratios in hot springs indicate long subsurface flow path and deep circulation (Fig. 3f). Some cold water samples (W19 and W30) are plotted close to the hot waters in Fig. 3, which is interpreted as being the result of local infiltration and mixing. High temperatures in the hot spring geothermal reservoirs and hot water–rock interaction make their hydrochemical features quite distinct from cold springs. This is particularly obvious when looking at some minor elements, such as Si, B, and Sr (Gupta et al. 2005). Generally, increasing temperatures causes an increase in minor element concentrations (Tarcan and Gemici 2003). These elements are relatively conservative and generally do not precipitate once dissolution has occurred. Cl, Si, B, and Sr concentrations are all higher in hot springs (Table 1). Some hot springs display higher mean Si concentrations (Fig. 5a). This can be attributed to flow through different lithologies, with different Si bearing minerals and different temperatures. The Si content in Qinerjeh hot springs (W21, W22, and W23) is lower than that of Thakhte-Solyman and Aqhdarreh hot springs (W12, W13, W17, and W42), suggesting more extensive silicate mineral dissolution. The lithology around Qinerjeh is made exclusively of metamorphic rocks, while in Thakhte-Solyman, some recharge water travels through sandstone, red marl, and travertine terrain, contacting carbonate minerals and mixing with fissure water during flow. Hot reservoir temperatures in Thakhte-Solyman and Aqhdarreh areas (see “Chemical geothermometry applications” section) may also contribute to more extensive silicate mineral weathering. According to the piper diagram, hot springs at Takhte-Soleyman field show higher Ca and SO_4 than Qinerjeh hot springs. The increase in HCO_3^- content could be explained by dissolution of limestone. Ca increase indicates that carbonate rocks comprise the main reservoir rocks for Takhte-Soleyman waters. Deep geothermal waters generally contain low SO_4^{2-}

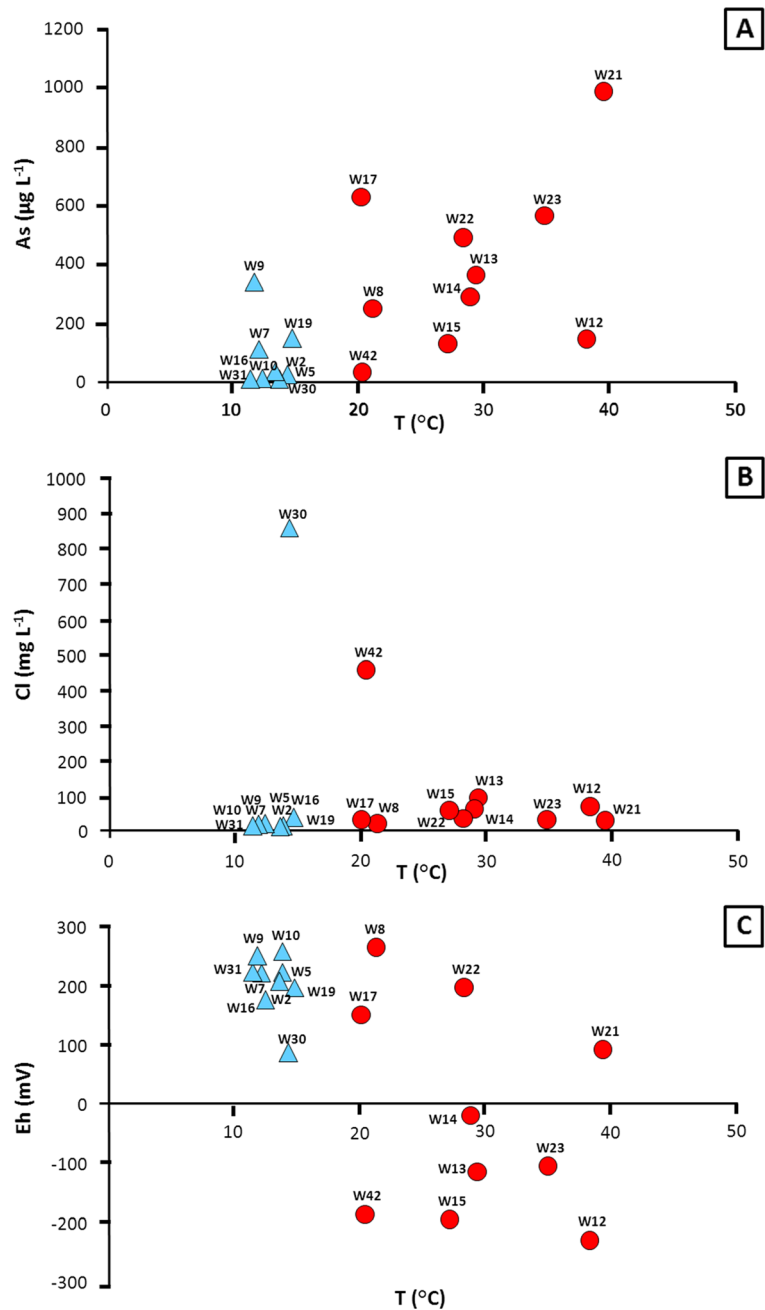
contents (<50 mg/l) (Nicholson 1993). Sulfate contents of water are quite high (9.66–700.49 mg/l) in the study area. High sulfate concentrations could be explained by dissolution of minerals like gypsum and/or oxidation of H_2S gas escaping from magma. Plots of discharge temperature versus As, Cl, and Eh (Fig. 4a–c) show that As and Cl demonstrate an approximately positive linear correlation with discharge temperature, whereas Eh has relatively negative correlation. This result demonstrates that hot springs with deep circulation and negative Eh display higher arsenic content. Sr concentrations increase with increasing Cl^- , indicating accumulation during water–rock interaction along water flow paths (Fig. 5b), and highlight differences in lithology. In the Thakhte-Solyman field, higher Sr concentrations and its correlation with Ca indicate mixing with carbonate water. Since Ca and Sr readily substitute in carbonate minerals, they likely have a common source (Cartwright and Weaver 2005). The relationship between B and Cl concentrations can be used to evaluate mixing between hot and cold waters (Inguaggiato et al. 2000). Cl versus B concentrations in the two water groups illustrate two distinct mixing trends (Fig. 5c), which suggests that both ions are behaving conservatively and that there is a direct hydraulic connection between hot and cold water systems. Minor and trace element concentrations are relatively higher in thermal waters because of the reservoir rock leaching.

The Cl-B- SO_4 plot (Fig. 6) also shows a clear distinction between the cold and thermal waters, indicating that the latter have more interaction with rocks. Thermal waters show high concentrations of B, a fact that is probably related to the high temperature leading to enhanced water–rock interaction and leaching of boron (Dotsika et al. 2006).

Chemical geothermometry applications

The thermal waters of Takab geothermal area were evaluated in the Na-K-Mg ternary diagram proposed by Giggenbach (1988) and the Na-K-Ca-Mg diagram proposed by Giggenbach and Corrales (1992). According to Na-K-Mg ternary diagram, Takab thermal waters fall in the immature water field (Fig. 7), indicating disequilibrium with the reservoir rocks, and are probably dominated by rock dissolution, mixing with cold groundwater, and ion exchange. Therefore, the results obtained from the cation geothermometers should be taken into account as doubtful. Also,

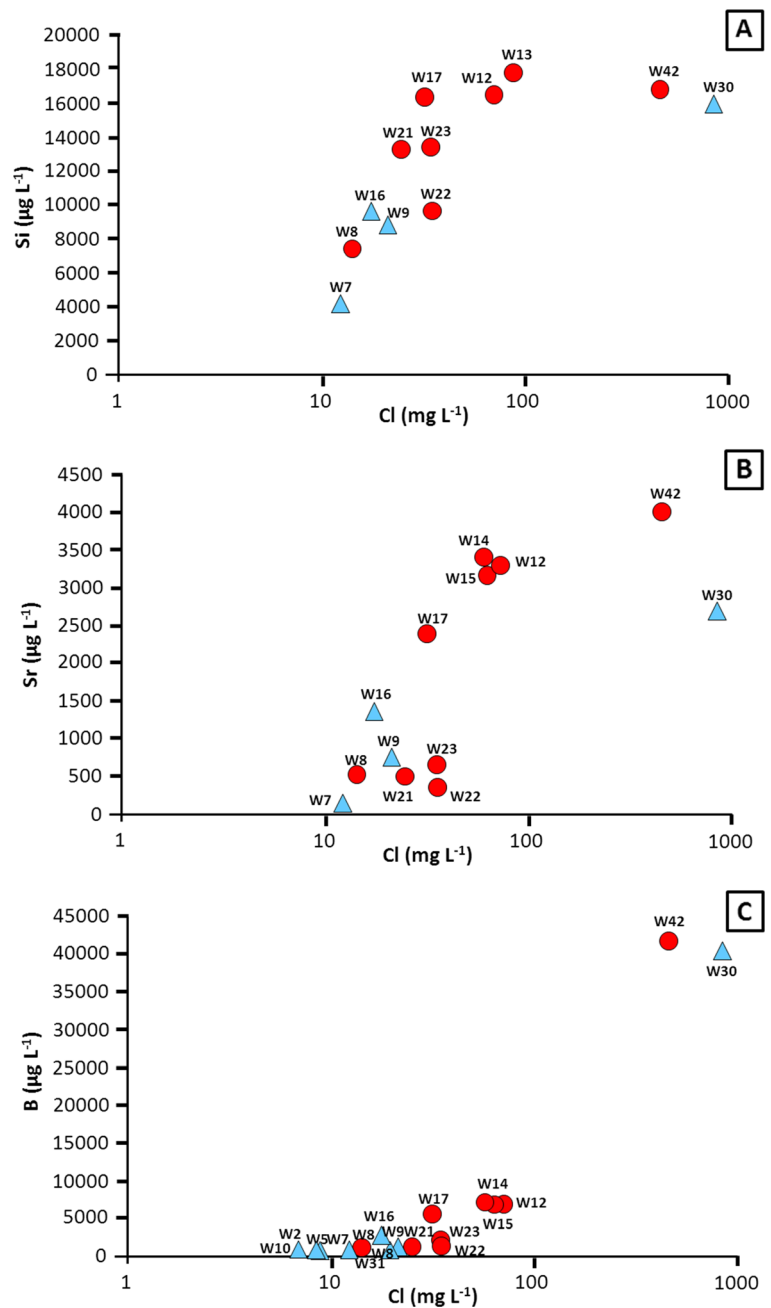
Fig. 4 Plots of As (a), Cl (b), and Eh (c) versus discharge temperature in sampled waters (symbols as in Fig. 3)



geothermometers based on Mg/Li (Kharaka and Mariner 1989) give lower reservoir temperatures than that of their discharging temperatures while Na/Li (Kharaka and Mariner 1989) give high reservoir temperatures, so these two geothermometers are also unreliable for the Takab geothermal fields. However, chemical analyses of thermal waters were used to estimate the reservoir temperature of Takab springs using several silica geothermometers. The results obtained are

presented in Table 2. Since silica geothermometer is based on absolute concentration rather than concentration ratios, it is affected by boiling and dilution more than the cation geothermometers. Some results are unreal since they are lower than the measured surface temperatures or they are too high. Some silica geothermometers (i.e., amorphous silica, α -cristobalite, and β -cristobalite) give unreasonable temperatures. The quartz geothermometers yield reservoir temperatures

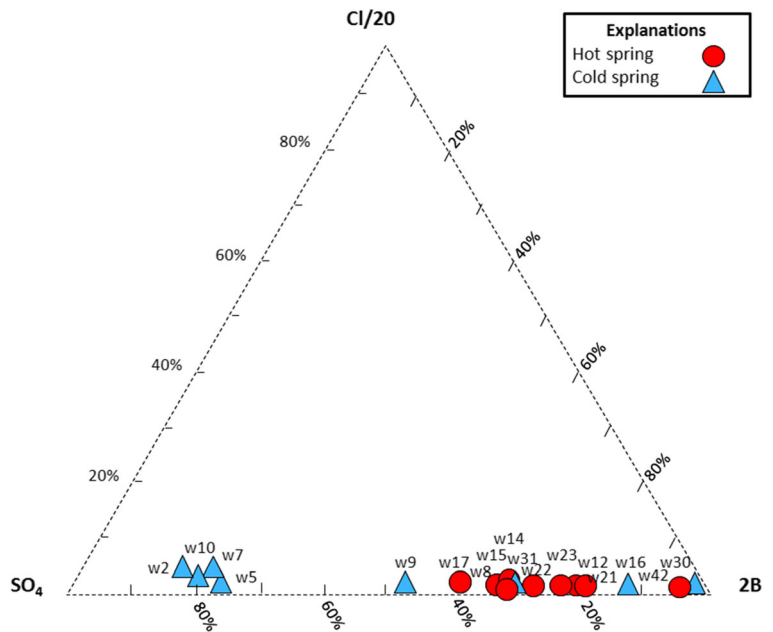
Fig. 5 Plots of Si (a), Sr (b), and B (c) versus Cl concentrations in sampled waters (symbols as in Fig. 3)



ranging from 35.33 to 91.82 °C. Chalcedony geothermometers compared with quartz geothermometers display relatively low temperatures between 25.15 and 58.66 °C. According to quartz geothermometers, reservoir temperatures of spring having limestone, marl, and volcanic reservoir rocks (Takhte-Soleyman and Aqdarreh fields) are from 39 to 91.8 °C. In addition, reservoir temperatures of other thermal waters with metamorphic reservoir rocks

(Qinerjeh field) also range from 45 to 81.8 °C. The increase in reservoir temperature is also related to high geothermal gradient due to volcanic and sedimentary basement rocks in the study area. Plotting silica and K-Mg equilibration temperatures may also be used to estimate reservoir temperatures in an environment occupied by a slow moving, single liquid phase, before the onset of boiling (Giggenbach et al. 1994). Allowing for some silica loss from the water, the maximum

Fig. 6 Cl-B-SO₄ ternary diagram



temperature indicated by this method for Takhte-Soleyman reservoir is 80 °C (Fig. 8). Reservoir temperatures for Qinerjeh field indicated by plotting log (K²/Mg) versus log (SiO₂) for the thermal waters (Fig. 8) are generally lower, ranging from 35 to 40 °C, suggesting that these waters have resided at lower temperatures for extended periods of time before emerging at the surface. The lower-temperature HCO₃-type waters in both fields are plotted at considerably lower temperatures. In the plot of Fig. 8, the Takhte-Soleyman data indicate equilibria between two SiO₂ species. It may be

assumed that both quartz species occur at least in the Takhte-Soleyman reservoir, while it might be different for the Qinerjeh reservoir. SiO₂ patterns in the two fields (Fig. 8) suggest that silica geothermometers may yield valid temperatures. Unfortunately, the predicted temperatures generally show a wide dispersion even when applying a single geothermometer in a geothermal field. Many reasons have been proposed to justify the discrepancies, including gain or loss of steam phase in the reservoir, mixing of different types of fluids, re-equilibration during ascent to the surface, and

Fig. 7 Water–rock equilibration for thermal and cold springs (Na, K, and Mg concentrations in mg kg⁻¹) (Giggenbach 1988; Giggenbach and Corrales 1992)

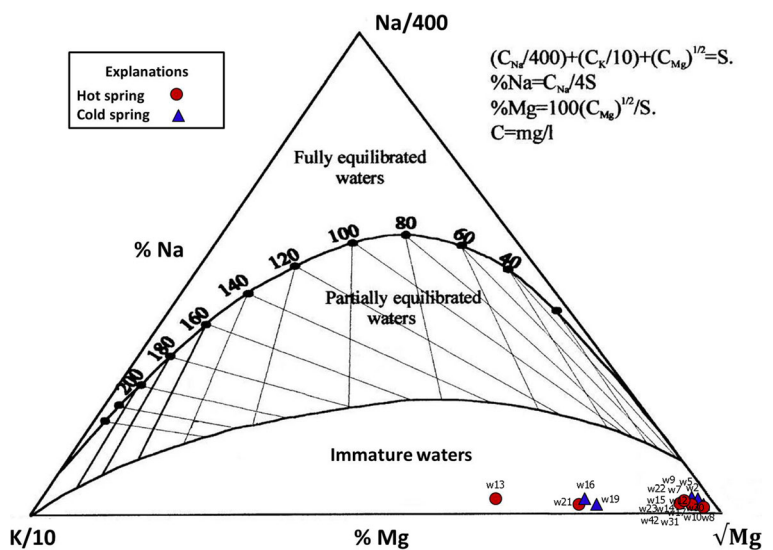


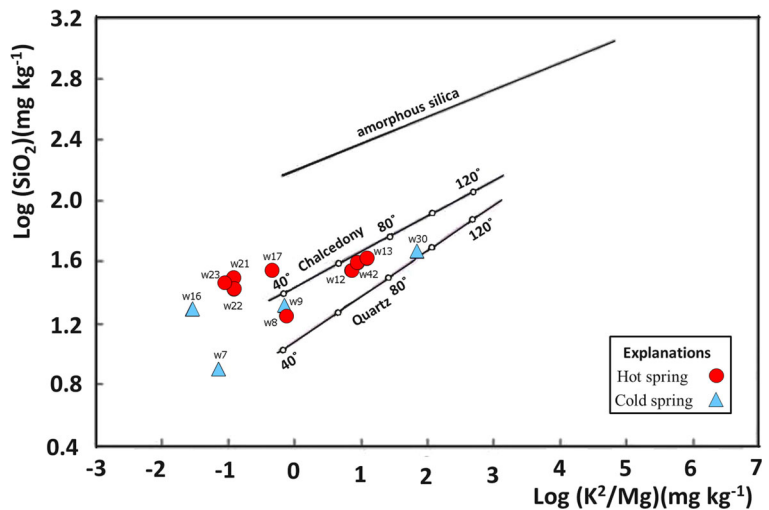
Table 2 Geothermometry results for water samples from Takab geothermal field

Geothermometry	W31	W9	W7	W16	W2	W10	W5	W30	W19	W42	W17	W8	W15	W14	W13	W12	W22	W23	W21
Discharge temperature (°C)	11.5	11.8	12.2	12.5	13.6	13.8	13.9	14.4	14.8	20.4	20.1	21.2	27.1	28.9	29.3	38.2	28.2	34.8	39.4
Quartz ^a	N/D	65.29	35.33	64.56	N/D	N/D	N/D	84.65	N/D	89.09	86.01	57.44	N/D	N/D	89.43	85.88	70.44	76.58	78.01
Quartz (maximum steam loss) ^a	N/D	70.59	43.71	69.95	N/D	N/D	N/D	87.64	N/D	89.78	88.83	63.61	N/D	N/D	91.82	88.72	75.15	80.57	81.83
Chalcedony ^a	N/D	33.28	2.54	32.53	N/D	N/D	N/D	53.58	N/D	56.17	55.02	25.15	N/D	N/D	58.66	54.89	38.65	45.09	46.59
α -cristobalite ^a	N/D	16.05	<0	15.36	N/D	N/D	N/D	34.68	N/D	37.05	36.01	8.57	N/D	N/D	39.33	35.88	20.99	26.89	28.27
β -cristobalite ^a	N/D	<0	<0	<0	N/D	N/D	N/D	<0	N/D	<0	<0	<0	N/D	N/D	<0	<0	<0	<0	<0
Amorphous silica ^a	N/D	<0	<0	<0	N/D	N/D	N/D	<0	N/D	<0	<0	<0	N/D	N/D	<0	<0	<0	<0	<0
Na-K ^a	291.46	357.72	<150	246.17	257.42	<150	241.15	257.85	173.25	253.96	194.85	386.36	207.39	196.31	345.12	328.65	257.42	257.42	243.61
Na-K-Ca ^a	<0	21.18	2.43	<0	<0	<0	<0	191.25	18.42	71.29	17.86	15.9	16.79	17.82	53.24	48.02	2.66	<0	0.11
Na-K-Ca-Mg ^b	<0	<0	>350	<0	<0	>350	<0	>350	<0	>350	>350	<0	>350	>350	>350	>350	<0	<0	<0
Mg-Li ^b	28.26	1.61	<0	33.6	25.56	13.24	37.67	74.16	N/D	78.82	46.44	3.4	57.06	52.75	N/D	51.85	16.83	26.71	28.74
Na-Li ^b	298.38	177.4	31.29	331.43	287.52	123.25	338.76	218.51	N/D	301.45	230.54	194.82	270.28	259.4	N/D	268.45	211.24	259.58	245.33

N/D not measured

^aFournier (1981)^bKharaka and Mariner (1989)

Fig. 8 Plot of $\log(\text{SiO}_2)$ versus $\log(\text{K}^2/\text{Mg})$, concentrations in mg kg^{-1} . The lines represent simultaneous attainment of equilibrium for the systems involving silica and K-Mg (Giggenbach and Glover 1992)



precipitation-dissolution (Verma 2001). Therefore, geothermometers and saturation indices should be assessed together to determine the reservoir temperature.

Mineral saturation states

Mineral saturation indices of hydrothermal minerals that are likely to be present in the reservoir of Takab geothermal system were calculated at measured surface temperatures using PHREEQC computer code (Parkhurst and Appelo 1999). The results are presented in Table 3. Gypsum and anhydrite are under saturated in all spring waters, indicating that dissolution of SO_4 is still going on in the reservoir. Calcite, dolomite, aragonite (except for W10, W22, W23, and W31), quartz, and chalcedony (except for W7, W8, W12, W21, W22, and W23) minerals are oversaturated or nearly in equilibrium at discharge temperatures. Muscovite, kaolinite, and K-feldspar minerals are supersaturated. Increasing SI values in Takab area, where carbonate and volcanic rocks, gneiss, and schist constitute the reservoir rocks, indicate that the reservoir rocks have influenced the chemical composition of springs and also point to a long time residence of water in the reservoir rocks. The equilibrium state between water and many mineral phases is a function of temperature (Reed and Spycher 1984). If the equilibrium lines of a group of predicted minerals converge, it indicates a temperature corresponding to the most likely reservoir temperature. Thus, saturation indices can be used as geothermometers (Davraz 2008). To evaluate the equilibrium states of some hydrothermal minerals at different temperatures, the temperature was changed taking

into account the hydrogen mass balance (Kharaka et al. 1988) and then saturation indices were recomputed. The mineral saturation indices versus temperature for hot springs are shown in Fig. 9. Due to the fact that waters in Takab area have high carbonate contents, the temperatures obtained from the equilibration of carbonate minerals such as calcite, dolomite, and aragonite were ignored in determining the best equilibrium temperatures. The mineral saturation indices of anhydrate, kaolinite, magnesite, muscovite, K-feldspar, and quartz minerals move toward zero (SI = 0) in the range of 60 to 92 °C for Takhte-Soleyman field (Fig. 9a–d). For Qinerjeh field, saturation indices with respect to kaolinite, magnesite, muscovite, and quartz minerals tend to get closer to zero around the temperature range of 60 to 80 °C (Fig. 9e–g). The Aqdarreh field attains equilibrium with albite, K-feldspar, kaolinite, muscovite, and quartz minerals in the temperature range of 70 to 90 °C (Fig. 9h). Gypsum is undersaturated in all collected waters, while dolomite and calcite are oversaturated. As mentioned, in the mineral saturation versus temperature diagrams, some minerals approach zero at various temperatures. Convergence of equilibrium lines (SI = 0) of a group of predicted minerals indicates the most likely reservoir temperature (Davraz 2008). The assessment of the saturation indices of the minerals indicated in Fig. 9 gives a reservoir temperature between 60 and 92 °C for Takab geothermal area. These values are compatible with chemical geothermometer results (Table 2). The fluid–mineral equilibrium in Takab geothermal area is also investigated by the activity diagrams. These diagrams are based on the estimation of the alteration minerals, which are formed as a result of water–rock interactions.

Table 3 Calculated saturation index (SI) for hot and cold springs from Takab geothermal field

Sample	Anhydrite	Aragonite	Calcite	Dolomite	Gypsum	Magnesite	Chalcedony	Kaolinite	Muscovite	Quartz	Albite	Analcime	K-Feldspar
W31	-2.23	-0.25	-0.11	0.46	-1.92	-1.14	N/D	N/D	N/D	N/D	N/D	N/D	N/D
W9	-1.92	0.19	0.33	1.67	-1.61	-0.37	0.2	4.59	6.53	0.48	-0.63	-1.12	1.96
W7	-2.84	0.07	0.22	0.8	-2.53	-1.12	-0.14	3.35	4.43	0.14	-0.98	-1.17	0.42
W16	-2.1	0.04	0.18	1.3	-1.8	-0.58	0.22	4.36	5.75	0.5	-0.71	-1.22	1.45
W2	-2.94	0.25	0.39	1.38	-2.64	-0.7	N/D	N/D	N/D	N/D	N/D	N/D	N/D
W10	-2.86	-0.23	-0.08	-0.11	-2.57	-1.72	N/D	N/D	N/D	N/D	N/D	N/D	N/D
W5	-2.46	0.24	0.38	1.68	-2.17	-0.39	N/D	N/D	N/D	N/D	N/D	N/D	N/D
W30	-1.64	0.27	0.42	1.53	-1.36	-0.57	0.4	5.19	7.63	0.68	0.67	-0.04	2.86
W19	-1.14	0.18	0.33	1.45	-0.85	-0.56	N/D	N/D	N/D	N/D	N/D	N/D	N/D
W42	-1.03	0.61	0.75	2.37	-0.8	-0.04	0.32	5.79	8.38	0.59	0.75	0.1	2.84
W17	-0.7	0.68	0.83	2.08	-0.44	-0.42	0.35	5.42	7.6	0.63	0.68	0.0	2.51
W8	-2.06	0.39	0.53	2.0	-1.84	-0.18	-0.07	3.79	5.24	0.2	-1.6	-1.83	0.91
W15	-0.6	0.36	0.5	1.37	-0.44	-0.75	N/D	N/D	N/D	N/D	N/D	N/D	N/D
W14	-0.54	0.91	1.06	2.65	-0.4	-0.01	N/D	N/D	N/D	N/D	N/D	N/D	N/D
W13	-0.81	0.8	0.95	2.46	-0.67	-0.09	0.15	4.02	6	0.42	-0.4	-0.86	1.86
W12	-0.77	0.58	0.73	2.12	-0.72	-0.15	-0.03	4.31	6.02	0.23	-0.86	-1.15	1.21
W22	-1.8	-0.02	0.13	0.98	-1.65	-0.75	-0.1	3.52	4.11	0.17	-1.97	-2.16	-0.02
W23	-1.56	-0.09	0.06	0.8	-1.47	-0.82	-0.07	4.13	4.6	0.2	-1.94	-2.16	-0.1
W21	-1.56	0.0	0.14	0.9	-1.51	-0.78	-0.15	3.06	3.17	0.11	-2.33	-2.47	-0.62

N/D not measured

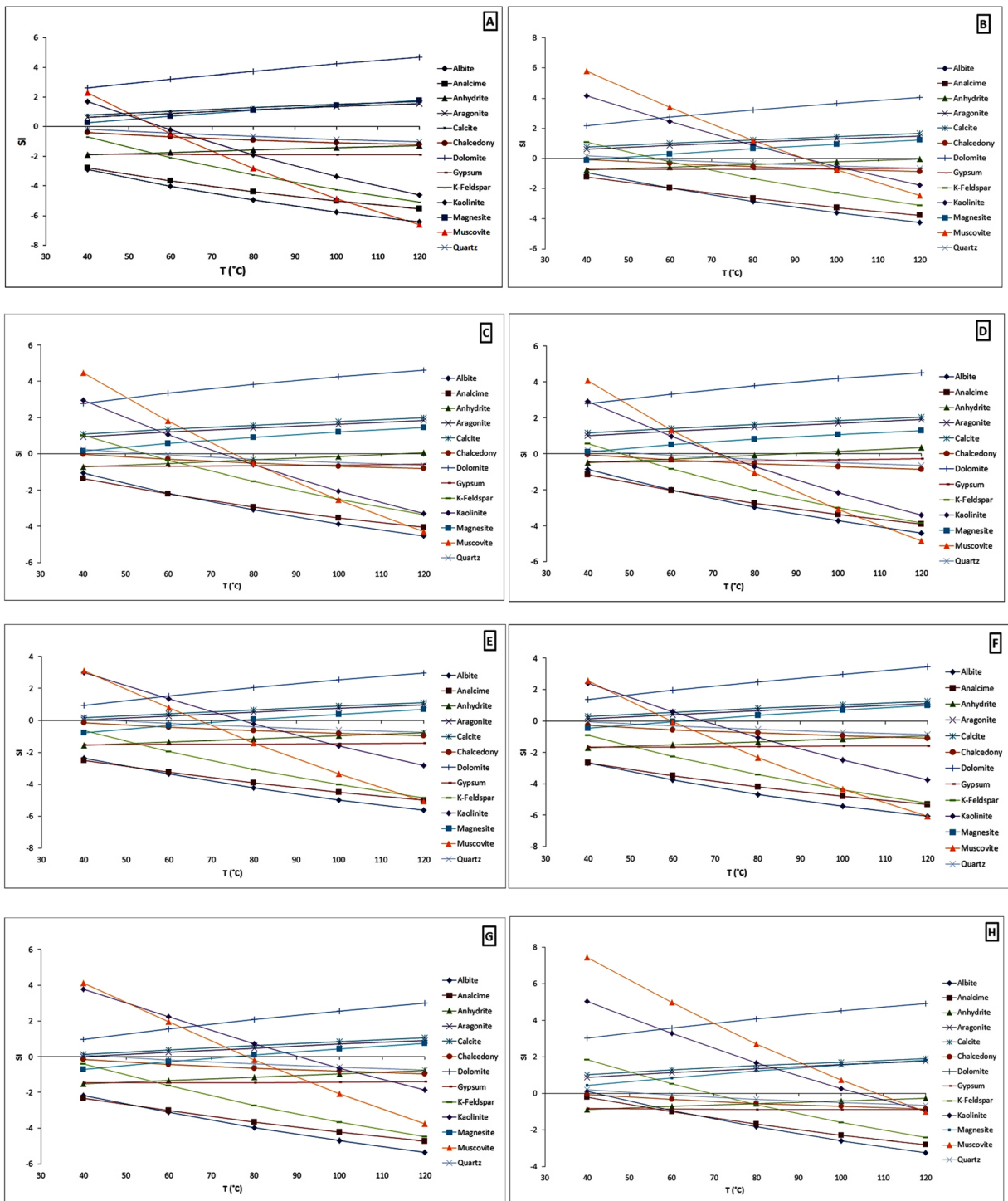
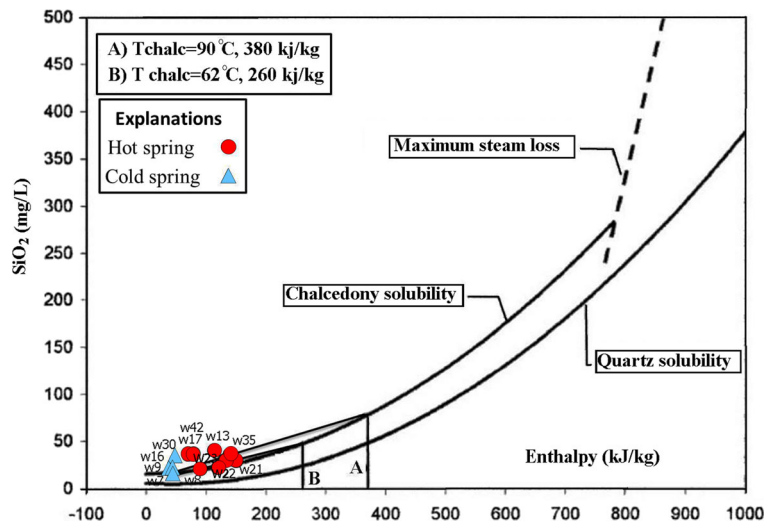


Fig. 9 Mineral equilibrium diagrams of hot waters, Takhte-soleyman (a–d), Qinerjeh (e–g), and Aqdarreh (h) fields

In the activity diagrams, constructed by Mutlu (1998), illustrations of phase relations between kaolinite, K-feldspar, albite, paragonite, and muscovite minerals were investigated at 100 and 125 °C (Fig. 10). Two

different systems were considered in the activity diagrams. The systems are $\text{Na}_2\text{O}-\text{K}_2\text{O}-\text{Al}_2\text{O}_3-\text{H}_2\text{O}$ as a function of $\log (a\text{Na}^+/\text{aH}^+)$ and $\log (a\text{K}^+/\text{aH}^+)$ and $\text{CaO}-\text{Al}_2\text{O}_3-\text{K}_2\text{O}-\text{H}_2\text{O}$ as a function of $\log (a\text{Ca}^{+2}/\text{aH}^+)$

Fig. 11 The silica-enthalpy mixing model for hot and cold springs from the Takab geothermal field



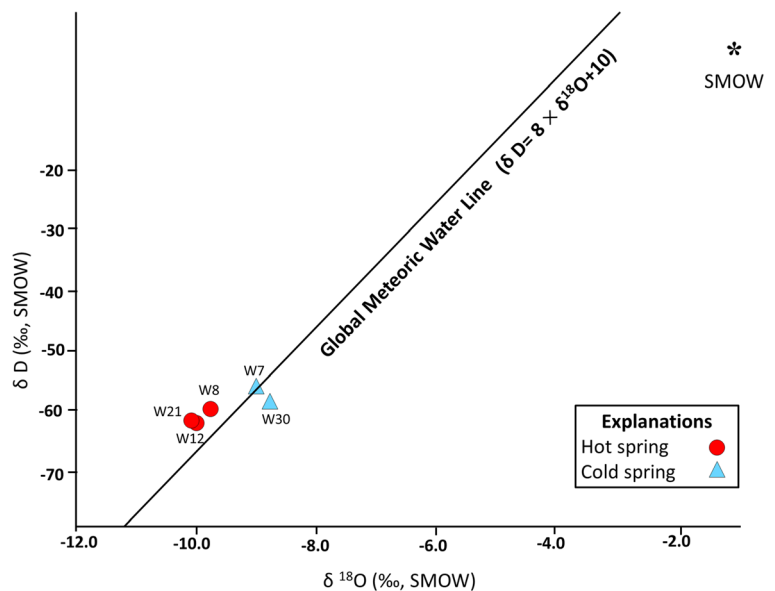
into consideration almost all the samples. The water enthalpies at the intersection of line A and line B with the chalcedony solubility curve are 260 and 380 kJ/kg, respectively, corresponding to estimated reservoir temperatures of 62 and 90 °C.

Isotopic composition of water samples

Environmental isotope data (¹⁸O and ²H stable isotopes) were measured at representative sampling points to provide useful information on sources of water and processes in the area. The relationship between the $\delta^{18}\text{O}$ and $\delta^2\text{H}$ values is plotted in Fig. 12, which also shows

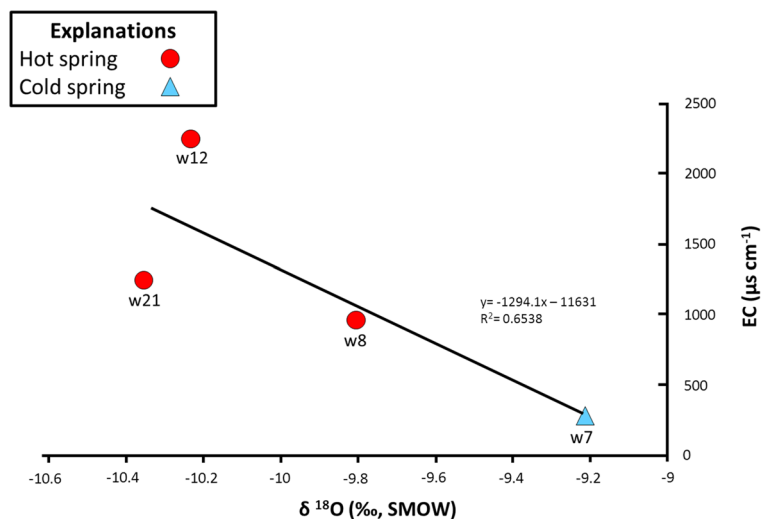
the Global Meteoric Line ($\delta\text{D}=8 \delta^{18}\text{O}+10$) of Craig (1961). Figure 12 shows that the $\delta^{18}\text{O}$ and δD values range from -9.8 to -10.35 ‰ and -59.92 to -63.25 ‰, respectively, for hot springs. For cold springs, the values vary from -8.8 to -9.22 ‰ and -57.15 to -59.61 ‰, respectively (Table 1). Cold spring samples plot on the Global Meteoric Line reflects their meteoric origin. Overall, the stable isotopic data indicate that Takab geothermal waters are of a meteoric origin with the deeply circulating meteoric waters over long residence times in the geothermal systems. The meteoric water infiltrated along fractures and faults, heated, and then returned to the surface through hydrothermal conduits.

Fig. 12 Plot of δD and $\delta^{18}\text{O}$ compositions of thermal and cold springs



However, there is no significant enrichment in their $\delta^{18}\text{O}$ composition. $\delta^{18}\text{O}$ – $\delta^2\text{H}$ contents of hot springs are more negative than those of cold waters, although their temperature is higher. The oxygen-18 shift must result from the following processes: (1) exchanges of oxygen isotopes of geothermal waters with magmatic steams (CO_2 and H_2S) arise during the waning stages of Tertiary–Quaternary volcanic activity or (2) exchanges of oxygen isotopes of geothermal waters during the hydration of silicate minerals (Clark and Fritz 1997; Qin et al. 2005). Consequently, hot springs shift to the left on the $\delta^{18}\text{O}$ – $\delta^2\text{H}$ graph. Furthermore, more negative values of ^{18}O are considered to indicate a relatively high elevation of recharge area (Clark and Fritz 1997; Dotsika et al. 2010). It may be concluded from Table 1 that Qinerjeh hot springs are fed from higher elevations than the source of Takhte-Soleyman hot springs. The conductivity and total dissolved solid values provide a good indication of the interaction time between the water and reservoir rock. The results show that low EC values in cold springs indicate shorter interaction time with reservoir rocks. This is also partly due to the influence of groundwaters, which are often fresh and with low EC. In Fig. 13, plot EC versus oxygen isotope ($\delta^{18}\text{O}$) shows a negative correlation ($R^2 = -0.65$). Furthermore, ion concentrations increase from cold toward hot springs. While hot springs are represented by high EC values, the cold spring displays high $\delta^{18}\text{O}$ value. It must be emphasized that, although Qinerjeh hot spring (W21) originates in higher recharge areas, its ion concentration is lower than Takhte-Soleyman hot spring (W12) due to mixing with shallow cold groundwater.

Fig. 13 $\delta^{18}\text{O}$ and EC relationship of water samples



Conclusion

The main objectives of this paper were to study the chemical characteristics of thermal fluids from Takab geothermal field, determine the type and origin of the waters, and predict subsurface temperature. The waters in the study area are hosted by several rock types. Fractures and faults act as conduit for the circulation and ascent of thermal waters. Cold springs are Ca-HCO_3 type and characterize groundwater circulation at shallow depths. In contrast to the shallow environment, the SO_4 -rich, deeper thermal waters are $\text{Ca (SO}_4\text{)-HCO}_3$ and Ca-SO_4 type and undergo significant change in the baseline chemistry along flow lines with increasing residence time. TDS is higher in thermal spring due to longer flow paths and residence time and also water–rock interaction. Chloride is not a major component in thermal and cold springs, and its presence is likely derived from evaporative formations. Sulfate content of the thermal waters of Takab geothermal field is quite high due to dissolution of minerals like gypsum and/or oxidation of escaping H_2S gas from magma. The isotopic data show that the thermal spring and cold spring have a meteoric origin. All thermal waters fall in the field of immature waters in Na-K-Mg ternary diagram. Therefore, the silica geothermometers are appropriate to estimate the reservoir temperature. Assessment of geothermometers show that the reservoir temperatures in the Takab area can reach up to 90 °C. The fluid–mineral equilibrium in Takab area is also investigated with activity diagrams. Based on these diagrams, it is concluded that thermal waters are likely to form

kaolinite, K-feldspar, and muscovite as alteration products. The silica-enthalpy mixing model predicts a subsurface reservoir temperature between 62 and 90 °C. Subsurface temperature estimates using this method are compatible with other geothermometers. Although temperature pattern at depth in Takab geothermal field is well known, the thermal springs emerging in this area do not seem to originate from high-enthalpy systems (measured discharge enthalpy value is about 260 to 380 kJ/kg). The heat source is probably the higher geothermal gradient created by a magmatic intrusion, affected by faults in the Takab geothermal field. Meteoric water as a source descends down deep into the reservoir and is heated by the magma mainly by conduction and convective cells, where the vapor-dominated phase in turn heats the aquifer above and evolves into a steam-dominated system. The water rises up toward the surface as hot springs along the main fracture system and mixes with the groundwater.

Acknowledgments The authors would like to acknowledge the help of Shiraz University Research Committee for financially supporting this research. Thanks are also extended to the Shiraz University Medical Geology Research Center and Center of Excellence for Geology.

References

- Allison, A. W., Brown, D. S., Novo-Gradac, K. J. (1991). MINTEQA2/PRODEFA2, a geochemical assessment model for environmental systems: version 3.0 user's manual. U.S. Environmental Protection Agency Report EPA/600/3-91/021.
- Azizi, H., & Moinevaziri, H. (2009). Review of the tectonic setting of Cretaceous to Quaternary volcanism in northwestern Iran. *Journal of Geodynamics*, *47*, 167–179.
- Boni, M., Gilg, H. A., Balassone, G., Schneider, J., Allen, C. R., & Moore, F. (2007). Hypogene Zn carbonate ores in the Angouran deposit, NW Iran. *Mineralium Deposita*, *42*, 799–820.
- Cartwright, I., & Weaver, T. R. (2005). Hydrogeochemistry of the Goulburn Valley region of the Murray Basin, Australia: implications for flow paths and resource vulnerability. *Hydrogeology Journal*, *13*, 752–770.
- Clark, I. D., & Fritz, P. (1997). *Environmental isotopes in hydrogeology*. New York: Lewis Publishers.
- Craig, H. (1961). Isotopic variations in meteoric waters. *Science*, *133*, 1833–1834.
- Daliran, F. (2003). Discovery of 1.2 kg/t gold and 1.9 kg/t silver in mud precipitates of a cold spring from the Takab geothermal field, NW Iran. In D. Eliopoulos et al. (Eds.), *Mineral exploration and sustainable development* (pp. 461–464). Rotterdam: Millpress.
- Daliran, F. (2008). The carbonate rock-hosted epithermal gold deposit of Agdarreh, Takab geothermal field, NW Iran—hydrothermal alteration and mineralization. *Mineralium Deposita*, *43*, 383–404.
- Daliran, F., Pride, K., Walther, J., Berner, Z. A., & Bakker, R. J. (2013). The Angouran Zn (Pb) deposit, NW Iran: evidence for a two stage, hypogene zinc sulfide–zinc carbonate mineralization. *Ore Geology Reviews*, *53*, 373–402.
- Davraz, A. (2008). Hydrogeochemical and hydrogeological investigations of thermal waters in the Usak Area (Turkey). *Environmental Geology*, *54*, 615–628.
- Dotsika, E., Poutoukis, D., Michelot, J. L., & Kloppmann, W. (2006). Stable isotope and chloride, boron study for tracing sources of boron contamination in groundwater: boron contents in fresh and thermal water in different areas in Greece. *Water, Air, and Soil Pollution*, *174*, 19–32.
- Dotsika, E., Lykoudis, S., & Poutoukis, D. (2010). Spatial distribution of the isotopic composition of precipitation and spring water in Greece. *Global and Planetary Change*, *71*, 141–149.
- Favara, R. O., Grassa, F., Inguaggiato, S., & Valenza, M. (2001). Hydrogeochemistry and stable isotopes of thermal springs: earthquake-related chemical changes along Belice Fault (Western Sicily). *Applied Geochemistry*, *16*, 1–17.
- Fournier, R. O. (1981). Application of water geochemistry to geothermal exploration and reservoir engineering. In L. Rybach & L. J. P. Muffler (Eds.), *Geothermal systems, principles and case histories*. New York: Wiley.
- Fournier, R. O., & Potter, R. W. (1979). Magnesium correction to the Na–K–Ca chemical geothermometer. *Geochimica et Cosmochimica Acta*, *43*, 1543–1550.
- Giggenbach, W. F. (1988). Geothermal solute equilibria. Derivation of Na–K–Mg–Ca geothermometers. *Geochimica et Cosmochimica Acta*, *52*, 2749–2765.
- Giggenbach, W. F., & Corrales, R. S. (1992). The isotopic and chemical composition of waters and steam discharges from volcanic magmatic-hydrothermal systems of the Guanacoste Geothermal Province, Costa Rica. *Applied Geochemistry*, *7*, 309–332.
- Giggenbach, W. F., & Glover, R. B. (1992). Tectonic regime and major processes governing the chemistry of water and gas discharges from the Rotorua geothermal field, New Zealand. *Geothermics*, *21*, 121–140.
- Giggenbach, W. F., Sheppard, D. S., Robinson, B. W., Stewart, M. K., & Lyon, G. L. (1994). Geochemical structure and position of the Waiotapu geothermal field, New Zealand. *Geothermics*, *23*, 599–644.
- GSI, Geological Survey of Iran. (1999). Geological map of Iran 1: 100,000 series, Sheet 5463, Takht-e-Soleyman.
- Gupta, S. K., Deshpande, R. D., Agarwal, M., & Raval, B. R. (2005). Origin of high fluoride in groundwater in the North Gujarat–Cambay region, India. *Hydrogeology Journal*, *13*, 596–605.
- Inguaggiato, S., Pecoraino, G., & D'Amore, F. (2000). Chemical and isotopic characterisation of fluid manifestations of Ischia Island (Italy). *Journal of Volcanology and Geothermal Research*, *99*, 151–178.
- Karimzadeh Somarin, A., & Lentz, D. R. (2008). Mineralogy, geochemistry and fluid evolution of a fossil hydrothermal

- system in the Paleogene Mendejin volcanic sequence, East Azarbaijan, Iran. *Mineralogy and Petrology*, 94, 123–143.
- Kharaka, Y. K., & Mariner, R. H. (1989). Chemical geothermometers and their application to formation waters from sedimentary basins. In N. D. Naeser & T. H. McCulloh (Eds.), *Thermal history of sedimentary basins* (pp. 99–117). New York: Springer.
- Kharaka, Y. K., Gunter, W. D., Affarwall, P. K., Perkins, E. H., De Braal, J. D. (1988). SOLMINEQ 88: a computer program code for geochemical modelling of water-rock interactions. In *US Geological Survey Water Investigations Report* (pp. 88–4227).
- Larsen, D., Swihart, G. H., & Xiao, Y. (2001). Hydrochemistry and isotope composition of springs in the Tecopa basin, southeastern California, USA. *Chemical Geology*, 179, 17–35.
- Modabberi, S., & Moore, F. (2004). Environmental geochemistry of Zarshuran Au-As deposit, NW Iran. *Environmental Geology*, 46, 796–807.
- Möller, P., Rosenthal, E., Geyer, S., & Flexer, A. (2007). Chemical evolution of saline waters in the Jordan–Dead sea transform and in adjoining areas. *International Journal of Earth Sciences*, 96, 541–566.
- Mutlu, H. (1998). Chemical geothermometry and fluid-mineral equilibria for the Omer-Gecek thermal waters, Afyon area, Turkey. *Journal of Volcanology and Geothermal Research*, 80, 303–321.
- Naderi Siah Siah, Gh. (2013). Hydrogeochemistry of heavy metals and geothermometry in Qurveh-Takab axis hydrothermal springs. M.sc. thesis Shiraz University, Shiraz. 159 pp.
- Nicholson, K. (1993). *Geothermal fluids, chemistry and exploration techniques*. Berlin: Springer.
- Parkhurst, D. L., & Appelo, C. A. J. (1999). User's guide to PHREEQC (version 2)—a computer program for speciation, batch-reaction, one-dimensional transport, and inverse geochemical calculations. USGS Water-Resources Investigations Report pp. 99–4259.
- Qin, D., Turner, J. V., & Pang, Z. (2005). Hydrogeochemistry and groundwater circulation in the Xi'an geothermal field, China. *Geothermics*, 34, 471–494.
- Reed, M. H., & Spycher, W. H. (1984). Calculation of pH and mineral equilibria in hydrothermal waters with applications to geothermometry and studies of boiling and dilution. *Geochimica et Cosmochimica Acta*, 48, 1479–1492.
- Saki, A. (2010). Proto-Tethyan remnants in northwest Iran: geochemistry of the gneisses and metapelitic rocks. *Gondwana Research*, 17, 704–714.
- Sharifi, R., Moore, F., & Keshavarzi, B. (2014). Potential health risks of arsenic, antimony and mercury in the Takab geothermal field, NW Iran. *International Journal of Environmental Studies*, 71(3), 372–390.
- Stockli, D., Hassanzadeh, J., Stockli, L., Axen, G., Walöker, J. D., & Terrence, T. J. (2004). Structural and geochronological evidence for Oligo-Miocene intra-arc low-angle detachment faulting in the Takab–Zanjan area, NW Iran. *Geological Society of America Program*, 36, 319.
- Tarcan, G., & Gemici, Ü. (2003). Water geochemistry of the Seferihisar geothermal area, İzmir, Turkey. *Journal of Volcanology and Geothermal Research*, 126, 225–242.
- Trusdell, A. H., & Fournier, R. O. (1977). Procedure for estimating the temperature of a hot-water component in a mixed water by using a plot of dissolved silica versus enthalpy. *United States Geological Survey. Journal of Research*, 5, 49–52.
- Vengosh, A., Helvacı, C., & Karamandereci, İ. H. (2002). Geochemical constraints for the origin of thermal waters from western Turkey. *Applied Geochemistry*, 17, 163–183.
- Verma, M. P. (2001). *Silica solubility geothermometers for hydrothermal systems. Water–rock interaction* (pp. 349–352). Lisse: Swets and Zeitlinger.
- Warner, N. R., Kresse, T. M., Hays, P. D., Down, A., Karr, J. D., Jackson, R. B., & Vengosh, A. (2013). Geochemical and isotopic variations in shallow groundwater in areas of the Fayetteville Shale development, north-central Arkansas. *Applied Geochemistry*, 35, 207–220.